Rényi entropy perspective on topological order in classical toric code models

Johannes Helmes,[1] Jean-Marie Stéphan,[2] and Simon Trebst[1]
[1]*Institute for Theoretical Physics, University of Cologne, 50937 Cologne, Germany*
[2]*Max-Planck-Institut für Physik komplexer Systeme, 01187 Dresden, Germany*
(Received 20 July 2015; published 24 September 2015)

Concepts of information theory are increasingly used to characterize collective phenomena in condensed matter systems, such as the use of entanglement entropies to identify emergent topological order in interacting quantum many-body systems. Here, we employ classical variants of these concepts, in particular Rényi entropies and their associated mutual information, to identify topological order in classical systems. Like for their quantum counterparts, the presence of topological order can be identified in such classical systems via a universal, subleading contribution to the prevalent volume and boundary laws of the classical Rényi entropies. We demonstrate that an additional subleading $O(1)$ contribution generically arises for all Rényi entropies $S^{(n)}$ with $n \geqslant 2$ when driving the system towards a phase transition, e.g., into a conventionally ordered phase. This additional subleading term, which we dub connectivity contribution, tracks back to partial subsystem ordering and is proportional to the number of connected parts in a given bipartition. Notably, the Levin-Wen summation scheme, typically used to extract the topological contribution to the Rényi entropies, does not fully eliminate this additional connectivity contribution in this classical context. This indicates that the distillation of topological order from Rényi entropies requires an additional level of scrutiny to distinguish topological from nontopological $O(1)$ contributions. This is also the case for quantum systems, for which we discuss which entropies are sensitive to these connectivity contributions. We showcase these findings by extensive numerical simulations of a classical variant of the toric code model, for which we study the stability of topological order in the presence of a magnetic field and at finite temperatures from a Rényi entropy perspective.

DOI: 10.1103/PhysRevB.92.125144 PACS number(s): 65.40.gd, 89.70.Cf, 03.65.Vf, 05.10.Ln

I. INTRODUCTION

The ground states of interacting many-body systems can exhibit subtle forms of order such as the formation of long-range topological order or the emergence of spin-liquid physics [1], both in the quantum and classical world. Distilling the precise nature of these unconventional forms of order or even identifying their mere existence from, for instance, the ground-state wave function of a quantum many-body system is a highly nontrivial endeavor. This is particularly true if one tries to rely on conventional characterization approaches (often inspired by their experimental feasibility) such as the use of correlation functions. As it is oftentimes the case, the breakthrough to overcome these limitations has come by completely changing one's point of view, in this case by adopting an information theory perspective on the many-body system [2].

One core concept of quantum information theory is to consider the entanglement for a bipartition of the many-body system into two parts and to precisely map out its dependencies on the size and shape of the boundary separating the two parts. This idea has been pioneered by Bekenstein and Hawking [3] who in their description of black holes have introduced the entanglement entropy as a quantitative measure of entanglement and demonstrated its characteristic boundary law scaling. The best-known example of an entanglement entropy is the von Neumann entropy

$$S(A) = -\mathrm{Tr}(\rho_A \ln \rho_A), \tag{1}$$

where ρ_A is the reduced density matrix of subsystem A after tracing out subsystem B. By considering higher moments of the density matrix, one can embed the von Neumann entropy into a family of Rényi entropies

$$S_n(A) = \frac{1}{1-n} \ln\left(\mathrm{Tr}\left[\rho_A^n\right]\right), \tag{2}$$

where the index n typically is an integer $n \geqslant 2$ with the limes $n \to 1$ recovering the von Neumann entropy (1).

In contrast to thermal entropies, these entanglement entropies are not extensive, but show a prevalent scaling with the length ℓ of the boundary of the bipartition [2]

$$S_n(A) = a\ell + b \ln \ell - \gamma + O(1/\ell), \tag{3}$$

where in addition to the boundary law scaling of the first term we explicitly list the first two subleading terms. The logarithmic corrections arise from corner contributions for gapless phases or quantum critical points [4]. We will focus in the following on the $O(1)$ contribution γ that is typically associated with the topological entanglement entropy [5,6] for gapped two-dimensional phases, although such $O(1)$ contributions are also known to arise at quantum critical points reflecting geometrical aspects of the subsystem [4]. For a gapped system, a finite value of γ not only indicates the presence of topological order, but also allows to narrow down [7] the precise type of the underlying topological quantum field theory due to its universal character [5,6]. One way to calculate the entanglement entropy γ from Eq. (3) is to perform a careful scaling analysis for bipartitions of varying size, as it was done, for instance, in identifying the emergence of topological order in the ground state of the Heisenberg antiferromagnet on the kagome lattice [8,9]. Alternatively, one can compute the topological entanglement entropy using one of the summation schemes put forward by Levin and Wen [5] or Kitaev and Preskill [6] that consider a set of bipartitions of a system of fixed system size constructed in a way that all

 ©2015 American Physical Society

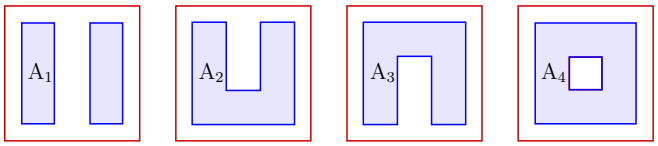

FIG. 1. (Color online) Illustration of the four bipartitions used in the Levin-Wen summation scheme to extract the topological entropy. The latter is calculated as $\gamma = -S(A_1) + S(A_2) + S(A_3) - S(A_4)$.

leading boundary and subleading corner contributions to the entanglement entropy precisely cancel. An illustration of the four bipartitions used in the Levin-Wen scheme is provided in Fig. 1.

A similar information theory perspective can also be taken to identify subtle orders in *classical* many-body systems, which will be the subject of this paper. In making this quantum to classical transition, we follow the work of Castelnovo and Chamon [10] and consider the Shannon entropy

$$S(A) = -\sum_{\{j_A\}} p_{j_A} \ln p_{j_A}, \tag{4}$$

where $\{j_A\}$ denotes the set of possible configurations of subsystem A in a bipartition of the system with statistical weights p_{j_A}. More generally, we can consider an entire family of classical Rényi entropies

$$S_n(A) = \frac{1}{1-n} \ln \left(\sum_{\{j_A\}} p_{j_A}^n \right), \tag{5}$$

where n again is a positive integer $n \geqslant 2$ and the limit $n \to 1$ recovers the Shannon entropy (4).

One key distinction of the classical versus quantum Rényi entropies is that the classical Rényi entropies follow a volume law

$$S_n(A) = c_V V_A + c_\ell \ell - \gamma + O(1/\ell), \tag{6}$$

where V_A now indicates the volume of partition A. The subleading $O(1)$ contribution γ again indicates the existence of topological order. For the classical toric code, which we will discuss in more detail in the following, its value of $\gamma = \ln 2$ resembles the result of the quantum version up to a factor of 2 as first discussed in Ref. [10] and recently expanded to a family of more general classical stringnet models [11].

In this paper, we carefully analyze this $O(1)$ contribution to the classical Rényi entropies when driving a system through a phase transition. As one particular example we consider the continuous phase transition from a topologically ordered to a conventionally ordered phase, which in the classical toric code can be driven by a magnetic field h. Our principal result is that for all higher-order Rényi entropies $S^{(n)}$ with $n \geqslant 2$ there is an additional constant term beyond the topological contribution for the intermediate coupling regime $h_c/n \leqslant h \leqslant h_c$. This additional contribution arises from partial subsystem ordering in this coupling regime. Because it is sensitive to the number of disconnected parts of these subsystems, we dub it a "connectivity contribution" to sharply distinguish it from the known topological contribution. To illustrate the generic, nontopological nature of this $O(1)$ connectivity contribution we also demonstrate its occurrence for the two-dimensional Ising model driven through its thermal phase transition. Finally, we come back to the classical toric code and round off our discussion by analyzing the finite-temperature behavior of the $O(1)$ contributions to classical Rényi entropies in a variety of settings.

The paper is organized as follows. We start with an introduction to the classical toric code in Sec. II. We then turn to the information theory perspective of classical many-body systems and (re)introduce classical Rényi entropies and related measures such as the mutual information and discuss their scaling behavior in Sec. III. In this section, we also motivate and discuss our main results from an analytical perspective. This is followed by a discussion of extensive numerical simulations in Sec. IV. We conclude with an outlook on the applicability of our results to quantum many-body systems and a discussion of the general shortcomings of Rényi entropies in Sec. V. The main body of the paper is complemented by an extensive Appendix, which gives a detailed exposition of the implementation of the replica technique to calculate the Rényi entropies. In particular, we comprehensively discuss how to combine nonlocal loop update techniques with the replica scheme.

II. CLASSICAL TORIC CODE MODEL

To set the stage for our analysis, we give a short introduction to the classical toric code model, which will serve as a paradigmatic example of a classical system with topological order in our subsequent discussion. The classical toric code is derived from its well-known quantum counterpart [12], which is captured by the Hamiltonian

$$H = -J_p \sum_{p \in P} \prod_{i=1}^{4} \sigma_{p_i}^x - J_v \sum_{v \in V} \prod_{i=1}^{4} \sigma_{v_i}^z, \tag{7}$$

where SU(2) spin-$\frac{1}{2}$ degrees of freedom located on the bonds of a square lattice are interacting via four-spin interactions around the plaquettes P and vertices V of the lattice. The two (commuting) terms energetically favor closed-loop configurations either in the σ_x or σ_z basis (which are dual to each other). The ground state of the Hamiltonian can then be written as a *loop gas*, i.e., an equal-weight superposition of all closed-loop configurations (in one of the two bases). We will work in the σ_z basis in the following.

The classical toric code is defined by interpreting the loop gas as a classical partition function, i.e., a partition sum to which all closed-loop configurations contribute equally. We can define a Hamiltonian for this classical system in terms of Ising variables located on the bonds of a square lattice as

$$H = -J_v \sum_{v \in V} \prod_{i=1}^{4} \sigma_{v_i}, \tag{8}$$

where a four-spin term for each vertex again favors even-parity spin alignment corresponding to closed-loop configurations. The low-temperature manifold of states for this classical Hamiltonian is thus again providing us with a loop gas. Like in the quantum model, we can define four distinct winding number parity sectors, which for a toroidal geometry (periodic boundary conditions) give rise to a fourfold degeneracy at

zero temperature, a hallmark of topological order also in the classical context. In the following, we will initially focus on this zero-temperature physics and impose a hard constraint on the system enforcing closed-loop configurations.

We can drive the classical toric code out of its topologically ordered phase by adding an external field term $-h\sum_{i=1}^{N}\sigma_i$ to the Hamiltonian that breaks the equal weightness of the closed-loop configurations constituting the loop gas. States with a higher total magnetization $m=\sum_{i=1}^{N}\sigma_i$ are preferred via statistical weights e^{hm} (in lieu of uniform weights 1 for the unperturbed loop gas). Since a majority of spins pointing up in the toric code lattice effectively shorten the length of the individual loops, we will also call h a *loop tension*. For sufficiently large strength this loop tension will drive a transition from the loop gas to a conventionally polarized state where all spins are aligned along the external field.

Note that in defining these statistical weights, we have not introduced the notion of temperature. We will return to this point in Sec. IV D where we discuss the role of open-loop defects arising at finite temperatures in Hamiltonian (8) and their interplay in the presence of a magnetic field.

A. Kramers-Wannier duality and the 2D Ising model

The zero-temperature physics of the classical toric code in a magnetic field can be mapped via a Kramers-Wannier duality [13] to a two-dimensional (2D) Ising model at finite temperatures, much like its quantum counterpart in a magnetic field can be mapped to a three-dimensional (3D) Ising model at finite temperatures [14]. To illustrate this mapping, consider an alternative set of Ising degrees of freedom μ_i located at the center of the plaquettes P of the original toric code model (see Fig. 2). For a given loop configuration $\{\sigma\}$ the values of these alternate Ising spins are chosen such that $\mu_i\mu_j=-\sigma_{\langle i,j\rangle}$ where sites i and j are nearest neighbors and $\sigma_{\langle i,j\rangle}$ is the spin on the toric code bond that separates plaquettes i and j. The magnetic field term of the toric code model thus induces an Ising interaction between the dual degrees of freedom. Note that loops in the toric code correspond to domain walls in the Ising model as illustrated in Fig. 2.

This duality between the toric code and the Ising model readily implies that the critical value of the loop tension h_c is directly related to the analytically known [15] critical value β_c of the finite-temperature transition in the Ising model

$$h_c^{\mathrm{TC}}=\beta_c^{\mathrm{Ising}}=\ln(1+\sqrt{2})/2\approx 0.440686\ldots .$$

It is also obvious that the mapping is unique up to a global flip of the Ising spins. In other words, the $\mathbb{Z}_2$ symmetry of the Ising model is lost in the toric code model [16].

The mapping also lets us understand the phase transition in the classical toric code as a continuous phase transition (in the 2D Ising universality class). In principle, one can of course track this transition (numerically) by measuring, for instance, the total magnetization m which serves as order parameter in the perspective of the Ising model. However, here we want to pursue a different direction and ask how other global quantities such as the Rényi entropies can be used to quantitatively track this phase transition.

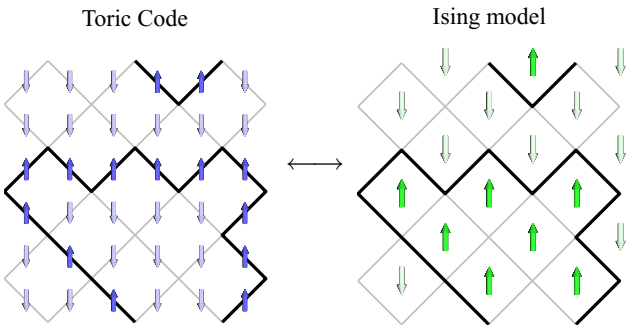

FIG. 2. (Color online) The well-known Kramers-Wannier duality [13] maps the classical toric code in a magnetic field to the 2D Ising model at finite temperatures.

III. CLASSICAL RÉNYI ENTROPIES

With the classical toric code at hand, we now direct our analysis towards the signatures of topological order in classical Rényi entropies. In this section, our emphasis will be mostly on an analytical perspective. To this end, we first provide a short introduction to the replica description of Rényi entropies. We then discuss the $O(1)$ contributions arising for the toric code model, in particular when driving the system through the field-induced phase transition to a topologically trivial phase.

A. Replica technique

Let us start our more detailed discussion of Rényi entropies by briefly laying out how one can calculate the Rényi entropies using the so-called *replica technique* [17]. The essential idea of this approach is to calculate the nth Rényi entropy from n replicas of the representation of the underlying many-body system.

This scheme was originally developed in the context of analytical calculations [17] of Rényi entropies for quantum field theories (on an n-sheeted Riemann surface) and later adapted to the analysis quantum many-body systems in condensed matter physics [18]. It is also directly amenable to numerical simulations and has first been ported to Monte Carlo simulations in the context of lattice gauge theories [19]. For quantum lattice models, the replica technique has first been reformulated in the context of stochastic series expansions in Ref. [20]. Subsequently, the replica technique has been adapted to various other flavors of quantum Monte Carlo including variational Monte Carlo [21], continuum-space path-integral Monte Carlo [22], determinantal Monte Carlo [23], fermionic continuous-time path-integral Monte Carlo [24], and hybrid Monte Carlo [25]. More recently, implementations of this replica technique have been envisioned for experimental settings [26], which has led to the first experimental measurement of Rényi entropies in an ensemble of ultracold atoms [27].

Here, we follow the work [28] by Iaconis and collaborators and adapt the replica technique to *classical* systems, an approach, which is again directly amenable to Monte Carlo simulations. We focus on the second Rényi entropy $S_2(A)$ and therefore consider two replicas of the system where the degrees of freedom in part A are precisely mimicking each other in the two replicas, while those in part B are allowed to

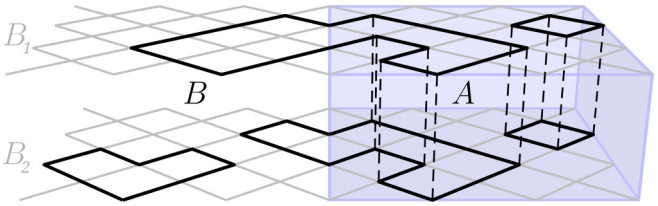

FIG. 3. (Color online) Illustration of the replica representation of the second Rényi entropy $S_2(A)$. Pictured are two replicas of the toric code model with a possible loop gas configuration superimposed. Similar to Fig. 2, the thick black lines represent up-pointing spins on the bonds of the lattice, while the down-pointing spins are not illustrated. Note that the loop configuration in the connected part A is identical in both replicas, while two independent loop configurations are allowed to occur in the two replicas of part B.

fluctuate independently for the two replicas (see Fig. 3 for an illustration). This replica representation of the Rényi entropy follows directly from writing the second-order Rényi entropy via its definition (5) and employing statistical weights $\exp(hm)$ to capture the effect of a finite magnetic field of strength h:

$$\begin{aligned} S_2(A) &= -\ln\left[\sum_{\sigma_A,\sigma_B,\sigma_{B'}} \left(p_{\sigma_A\cup\sigma_B}\right)\left(p_{\sigma_A\cup\sigma_{B'}}\right)\right] \\ &= -\ln\left[\sum_{\sigma_A,\sigma_B,\sigma_{B'}} \left(\frac{e^{h(m_A+m_B+m_A+m_{B'})}}{Z[h]^2}\right)\right] \\ &\equiv -\ln\left[\frac{Z[A,2,h]}{Z[h]^2}\right]. \end{aligned} \tag{9}$$

Here, we have introduced the partition function $Z[h]$ of the total system in the presence of a magnetic field of strength h. The second partition function $Z[A,2,h]$ captures a setting in which subsystem A is subject to a magnetic field of strength $2h$, i.e., *twice* the strength of the applied magnetic field, while the two replicas for subsystem B are subject to a magnetic field of strength h.

This replica representation of arbitrary Rényi entropies with $n \geqslant 2$ is then obtained in a straightforward manner. In general, one encounters partition functions of the form $Z[A,n,h]$ describing a system, in which subsystem A experiences a magnetic field of strength nh, while being coupled to n independent replicas of subsystem B, each experiencing a magnetic field of strength h.

B. Topological entropy and connectivity contribution

As mentioned already in the Introduction, the classical Rényi entropies generically follow a volume law as given in Eq. (6) augmented by a subleading boundary law and $O(1)$ contributions indicative of topological order. We will concentrate on precisely these $O(1)$ contributions in the following. To extract them from the Rényi entropy we employ the Levin-Wen summation scheme [5] considering the four bipartitions A_1, A_2, A_3, and A_4 illustrated in Fig. 1. Adding up the Rényi entropies of these four bipartitions as

$$\Delta S = -S_2(A_1) + S_2(A_2) + S_2(A_3) - S_2(A_4), \tag{10}$$

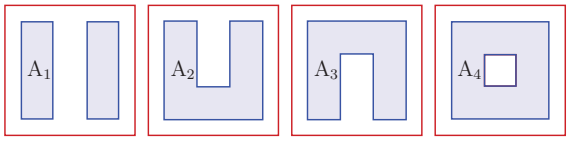

topological ($h < h_c/2$)				
γ^A	0	0	0	$\ln 2$
γ^B	$\ln 2$	0	0	0
connectivity ($h_c/2 < h < h_c$)				
γ^A	$2\ln 2$	$\ln 2$	$\ln 2$	$2\ln 2$
γ^B	$2\ln 2$	$\ln 2$	$\ln 2$	$2\ln 2$

FIG. 4. (Color online) Constant contributions to the second Rényi entropy in the topologically ordered phase of the classical toric code model in a magnetic field of strength h for the different bipartitions in the Levin-Wen scheme. For simplicity, $n = 2$ is shown.

we note that all volume, boundary, and possible corner contributions to the Rényi entropies precisely cancel so that ΔS provides us with a direct measurement of the remaining $O(1)$ contributions. Following the work of Ref. [11], we first note that in the classical context only the fourth bipartition in the Levin-Wen scheme contributes a nonzero *topological* contribution as listed in the Table of Fig. 4. It is this nonvanishing contribution which provides us with a topological entropy of precisely $\gamma = \ln 2$ for the unperturbed classical toric code as originally shown by Castelnovo and Chamon [10].

We now consider the effect of a finite-loop tension (or magnetic field). From the Kramers-Wannier duality to the Ising model we already know that only when the loop tension reaches the critical value $h_c = \ln(1+\sqrt{2})/2$ topological order in the system is destroyed. When considering the regime $h < h_c$ from a renormalization group perspective, the effect of a loop tension renormalizes to zero in the thermodynamic limit and this physics should also be reflected in the entropy. One might thus be (mis)led to expect a constant $\gamma = \ln 2$ contribution to the classical entropy all the way up to the critical value h_c.

In fact, however, the situation turns out to be a bit more subtle for Rényi entropies. To get the topological entropy, it is mandatory that *all* replicas remain topologically ordered. But, as we have seen in the replica representation of the Rényi entropies in Sec. III A, one should think of the two subsystems being exposed to different strengths of the loop tension, e.g., for the second Rényi entropy one has field strengths $2h$ and h for subsystems A and B, respectively. This requires to refine our (renormalization group) perspective to consider *three* separate parameter regions.

When $h < h_c/2$, all replicas are in the topological phase. Here, the loop tension is an irrelevant perturbation (in a renormalization group sense), and the arguments of Ref. [10] apply. Hence, we expect a purely topological $O(1)$ contribution of $\gamma = \ln 2$ to be calculated by the Levin-Wen scheme.

When $h > h_c$, all replicas are in the ordered phase, with most spins pointing up. As can be understood by considering

the limiting case $h \to \infty$ with zero entropy, the four contribution of Eq. (10) become identical and the $O(1)$ contribution ΔS vanishes in the thermodynamic limit.

The intermediate region $h_c/2 < h < h_c$ is somewhat more delicate. Here, we have one replica A already in the ordered phase, while coupled to n replicas of B still in the topological phase. In case the bipartition leads to a single boundary (i.e., bipartitions A_2 and A_3) this generates an extra contribution $\ln 2/(n-1)$ to the entropy. In case the bipartition gives two separate boundaries (i.e., bipartitions A_1 and A_4, in which either subsystem A or B comes in two disconnected parts) the contribution becomes $2\ln 2/(n-1)$. We name this contribution *connectivity contribution*, as it has no topological origin and is instead sensitive to the disconnected parts in subsystem A or B. The various contributions to the entropy for each geometry are detailed in Fig. 4, specifying the situation of $n = 2$ for simplicity.

Adding up the individual contributions, the Levin-Wen summation scheme then yields

$$\Delta S = \begin{cases} \ln 2, & h < h_c/2 \\ \frac{n}{n-1}\ln 2, & h_c/2 < h < h_c \\ 0, & h > h_c \end{cases} \tag{11}$$

in the three different parameter regions.

This is one of the main results of this paper. It will be checked numerically for $n = 2$ and large system sizes in Sec. IV. Let us finally comment on the two special values $h = h_c/2$ and $h = h_c$. In that case, one or several of the replicas are exactly at the critical temperature in the language of the dual Ising model. These replicas are now governed by the Ising conformal field theory. It is known [29] that in the vicinity of the critical point, the corner contributions are enhanced to logarithmic terms $\propto \ln(L/a)$, where a is some microscopic cutoff and of the order of a lattice spacing. As is explained in Ref. [30], these logarithmic terms are canceled by the linear combination (10). However, there is no reason for all microscopic cutoffs to be the same. This means there is going to be an extra nonuniversal $O(1)$ contribution to ΔS arising in the vicinity of the critical points. Hence, we expect a nonvanishing, but nonuniversal value for ΔS exactly at the critical points $h = h_c/2$ and $h = h_c$.

IV. NUMERICAL SIMULATIONS

To complement the analytical perspective on Rényi entropies for the loop tension driven phase transition in the toric code, we will now turn to a discussion of extensive numerical simulations of this model.

A. Monte Carlo setup

We start our discussion of the numerical simulations by first outlining some aspects of our classical Monte Carlo setup, in particular with regard to the choice of bipartition, the numerical adaptation of the replica technique, as well as the implementation of nonlocal loop update techniques.

1. Bipartition

Let us first discuss our general choice for bipartitioning the system. A naive approach would probably cut along the lines of the square lattice and therefore also cut through spins. This is certainly not desirable, as it would also imply that some loop segments could run along the boundary of the bipartition (see also Fig. 2) and in general it would leave us wondering how to assign the degrees of freedom on the boundary to the respective subsystems. Instead, we choose to rotate the toric code lattice by 45° and perform diagonal cuts in a way such that each plaquette is cut symmetrically along each line of the bipartition. This is illustrated for subsystem A_4 in Fig. 5.

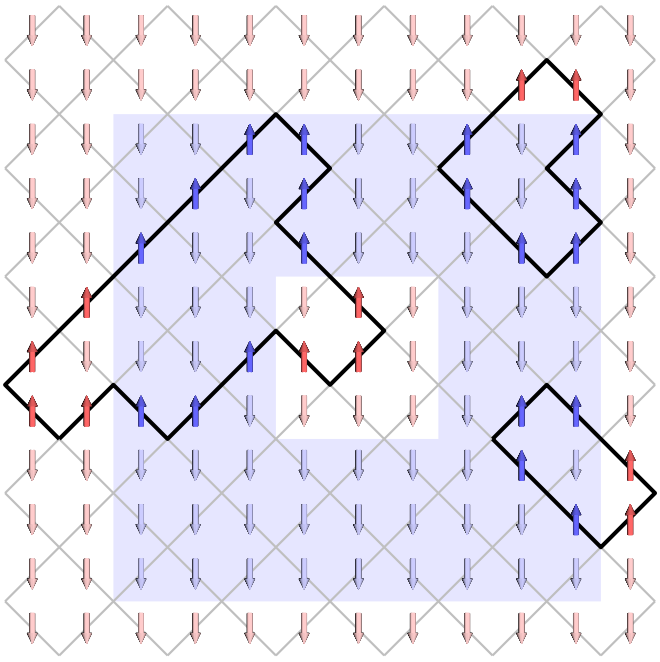

FIG. 5. (Color online) Fourth bipartition of the Levin-Wen scheme as an example of how the subdivision is performed. Spins in subsystem A are shown in blue, spins in B are in red. The loops are represented by thick black lines.

2. Replica technique

We employ two alternative approaches to implement the replica representation (9) and calculate the Rényi entropy from the ratio of the partition functions $Z[h]$ and $Z[A,2,h]$ as

$$S_2(A) = -\ln\left[\frac{Z[A,2,h]}{Z[h]^2}\right]$$

in a classical Monte Carlo setup.

The first approach uses the fact that for a given partition function, e.g., $Z[h]$, we have $\frac{\partial \ln Z[h]}{\partial h} = \langle m \rangle$ and we can thus obtain the entropy by performing an integration over the estimated values of the magnetization $\langle m \rangle$ for a dense range of parameters h. This method is an adaptation of the thermodynamic integration employed, e.g., in the context of thermal phase transitions [28,31].

The second approach is often referred to as *ensemble switching* [32] as it relates the ratio of the two partition functions $Z[h]^2$ and $Z[A,2,h]$ to the number of times one can switch between the two ensembles for a given sequence of configurations in a Markov chain. To this end, one samples configurations that belong to the system with partition function $Z[h]^2$, i.e., two copies of the full system. Noticing that

the configuration space of $Z[h]^2$ fully includes the one of $Z[A,2,h]$, we can readily estimate the relative weight of the two partition functions (needed for the above ratio) by simply counting how often a configuration in the Markov chain of the partition function $Z[h]^2$ also belongs to the one for partition function $Z[A,2,h]$. The ratio between the number of such coincidences and the total number of simulation steps is precisely $Z[A,2,h]/Z[h]^2$.

It turns out that neither of the two strategies is preferable for a wide range of system sizes. The thermodynamic integration needs a constant amount of individual simulations in order to densely cover the integration space, independently of the system size, while for the ensemble switching only a single simulation is needed. However, a common configuration of both $Z[h]^2$ and $Z[A,2,h]$ requires the full agreement of all spins in part A and thus becomes a rare event when part A is large, leading to a dramatic increase in simulation times to obtain small statistical errors. This drawback can be partially cured by a so-called increment trick [20], which subdivides the problem into individual simulations for subsets of a partition of A.

We find that thermodynamic integration typically outperforms the ensemble switching method for large systems (i.e., $L \gtrsim 48$), while the reverse is true for smaller sizes. As such, we employ both approaches in the following.

3. Loop updates

To efficiently sample the loop gas configurations constituting the partition function of the classical toric code nonlocal update techniques are an essential requirement. While such nonlocal update techniques, e.g., in the form of loop updates, are well known and widely employed, for instance, in the context of stochastic series expansions [33], the combination of these techniques with the replica technique has not been developed so far (neither in the context of quantum systems nor for classical loop models). The complication one faces when combining these two approaches is manifesting itself at the boundary of the bipartition where valid loop configurations must be sampled at all times. In particular, this implies that when iteratively building up the loop update the algorithm needs to branch out into multiple replicas, e.g., when building a loop starting from subsystem A and branching out into the independent subsystems $B_1, B_2, \ldots, B_n$ (see Fig. 3 for an illustration). One major technical achievement of this paper is the development of precisely such a (directed) loop update algorithm that *efficiently* samples replica-consistent loop gas configurations for closed loops as well as excited states with open loops. We refer to the Appendix for a detailed description of this update scheme and only want to briefly sketch the main ideas in this section.

In an initial strategy, we separate the tasks of identifying and accepting a new configuration. The first task is accomplished by performing an unbiased random walk that starts at an arbitrary vertex in the replicated lattice and continues through the lattice until it rejoins its initial vertex. If it enters the connected subsystem A, the random walk simultaneously traverses in both replicas and subsequently bifurcates at the boundary when transitioning back into the multiple independent replicas of subsystem B. If such bifurcations occur, we need to not only rejoin the first vertex, but also ensure that all open ends at these intermediate bifurcations are eventually turned into closed-loop configurations. Once a valid closed-loop structure has been identified, the statistical weight of the resulting new spin/loop configuration (in which all spins are flipped for all segments along the identified loop structure) is determined and the resulting configuration is accepted with Metropolis probability. This update procedure can easily be adapted to a case where also open-loop ends are allowed (a scenario relevant for finite-temperature simulations discussed in Sec. IV D). The probability for the emergence of a new pair of defects is simply included in the Metropolis selection.

A more advanced strategy already ensures the correct acceptance probability in the way it generates a new configuration. The random walk which samples a new loop in the lattice is no longer unbiased but *directed*, i.e., the direction of turns in the loop update depends on the local loop configuration at every vertex and is biased with certain statistical weights. Note that in our context the term *directed loop* refers to loops in the lattice and not in the imaginary-time expansion of worldline or SSE-type quantum Monte Carlo approaches. Also for this advanced strategy the update loop undergoes intermediate bifurcations if it exits subsystem A and we have to perform the walk until all open ends (including those occurring at the boundary between the two subsystems) are rejoined. Allowing for open-loop ends (e.g., in the finite-temperature simulations of Sec. IV D), this approach is readily modified by adding the possibility to stop the loop at a specific vertex and thereby creating an excitation.

For further details on these two approaches, in particular the detailed balance equations required to implement the directed loop updates, we refer to the extensive Appendix of this paper.

To obtain our simulation results, we used a combination of both algorithms since it turns out that the unbiased random walk strategy is more efficient for small loop tensions h, while the directed walk is performing better for intermediate to large loop tensions $h \gtrsim 0.3$.

B. Mutual information

We start our presentation of numerical results by first looking at the (Rényi) mutual information, a quantity that tracks long-range correlations between two parts of a many-body system. It is obtained from the Rényi entropies as

$$I_2(A:B) = S_2(A) + S_2(B) - S_2(AB). \tag{12}$$

Heuristically, the mutual information indicates how much information may be gathered about subsystem A by doing all possible measurements in subsystem B (and vice versa). Such an information retrieval about part A occurs in particular in the presence of long-range correlations, which mediate some of the information about subsystem A into subsystem B where it can be gathered. As such, we expect the classical mutual information to be finite in an ordered phase and easily distinguished from the vanishing value expected for a disordered phase. The mutual information has indeed proven to be a versatile indicator of phase transitions [28,34]; it is therefore natural to also consider it in the context of topological order as we will do in the following.

Before doing so, we note that contrary to the classical entropy, the mutual information obeys a *boundary* law

$$I_2(A:B) = c_\ell(\ell - 1) + a \tag{13}$$

as all bulk contributions are canceled by definition and I_2 is instead sensitive to subleading contributions to the Rényi entropies, which we have specified here as a boundary and a constant contribution.

Focusing on the boundary contribution first, note that we wrote a term proportional to $(\ell - 1)$ instead of the total length ℓ of the boundary. The reason for this reduced scaling form originates directly from the loop gas constraint that all loops need to be closed. As such, only an even number of loop segments is allowed to cross the boundary between the two subsystems A and B, i.e., specifying the loop occupation of $\ell-1$ bond segments along the boundary we can readily deduce the occupation of the last bond segment. This argument not only provides us with the $\ell - 1$ factor, but also readily determines the coefficient of the boundary contribution to be $c_\ell = \ln 2$. For further details of this argument, we refer to Ref. [11], in which classical loop gas (and string net) states have been extensively discussed from a combinatorial perspective.

Let us now turn to the subleading constant contribution a to the mutual information. This contribution can be readily calculated from the $O(1)$ contributions to the Rényi entropies as specified in the table of Fig. 4. Noting that for a half-torus bipartition as employed in our numerical simulations (see following), no topological $O(1)$ contributions are expected to occur, we directly probe the connectivity contributions to the entropies. We thus expect the constant contribution to the mutual information to be

$$a = \begin{cases} 0, & h < h_c/n \\ -\frac{1}{n-1}\ln 2, & h_c/n < h < h_c \\ 0, & h > h_c \end{cases}$$

for arbitary Rényi entropies with $n \geqslant 2$.

In our numerical setup for the classical toric code, we choose a symmetric bipartition of a quadratic lattice of size $L \times L$ with periodic boundary conditions (torus) where part A is precisely one half of the torus. The boundaries are two straight lines of length $\ell = L$. The symmetry of this bipartition readily implies $S_2(A) = S_2(B)$. Our results for the mutual information $I_2(A:B)$ are plotted in Fig. 6 for varying values of the loop tension h. Indeed, the illustrated behavior of the mutual information, rescaled by the length of the boundary, nicely confirms our expectation: In the loop gas limit of small loop tension, the data for different system sizes L collapse onto a single curve, which saturates at the expected value of $c_\ell = \ln 2$. For strong loop tension $h > h_c$ where the system is in a polarized state, the mutual information drops to zero as expected. Of interest is the intermediate regime $h_c/2 \leqslant h \leqslant h_c$, in which the mutual infomation first splits at $h_c/2$ for different system sizes, overshoots the value of $\ln 2$, and subsequently exhibits a crossing points at h_c. The behavior in the intermediate region can be traced back to the fact that subsystem A is effectively in the polarized state, which leads to an overestimation of the information to be gained about this state from the perspective of subsystem B.

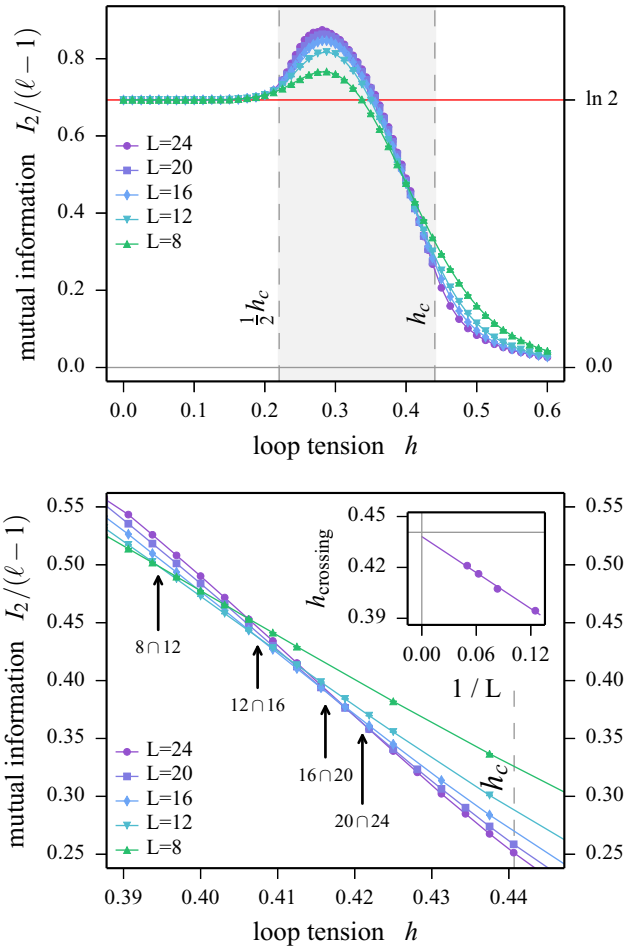

FIG. 6. (Color online) Top panel: mutual information I_2 of the classical toric code model with a magnetic field/loop tension h for varying system sizes. The gray shaded area indicates the intermediate regime $h_c/2 \leqslant h \leqslant h_c$. Bottom panel: zoom of the data near h_c illustrating the crossing points for different system sizes. The inset shows a scaling of the crossing points with inverse system size $1/L$ extrapolating well to the expected value of $h_c = \ln(1+\sqrt{2})/2 \approx 0.440686\ldots$ in the thermodynamic limit (indicated by the gray lines).

To understand why we see a splitting versus a crossing point at $h_c/2$ and h_c, respectively, it is worthwhile taking a look at the subleading contributions to the mutual information. To this end, we have fitted our numerical results for the mutual information for different system sizes to the expected scaling behavior of Eq. (13). Results for the obtained boundary coefficient c_ℓ and constant coefficient a are shown in Fig. 7. It is confirmed that the boundary coefficient c_ℓ attains a limiting curve which coincides with Fig. 6 in the thermodynamic limit. More interesting is the constant contribution a whose sign changes explain the splitting versus crossing points for different system sizes. In accordance with our expectation we see that this constant term does follow the behavior described in Eq. (14). In addition, we see that the coefficient a undergoes a sign change at h_c, which results in the crossing point of the mutual information [28]. In contrast, at $h_c/2$ it does not change signs but goes from zero to negative, which in turn yields the splitting of the mutual information (but not a crossing point).

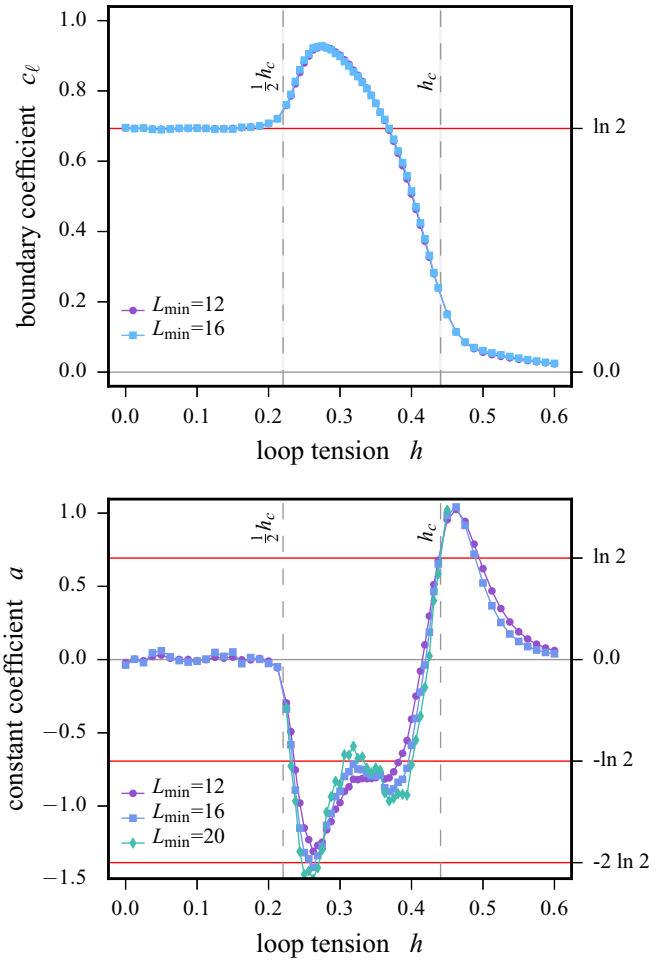

FIG. 7. (Color online) Contributions to the finite-size scaling of the mutual information for the classical toric code model with magnetic field/loop tension h. We fit the mutual information to the form $I_2(A:B) = c_\ell(\ell - 1) + a$ where ℓ is the length of the boundary of the bipartition. The top panel shows the boundary coefficient c_ℓ and the bottom panel the constant contribution a of this fit. Data are obtained from fitting system sizes $L_{\min} = 12$ to $L_{\max} = 24$ and $L_{\min} = 16$ to $L_{\max} = 24$, respectively. The gray shaded area indicates the intermediate regime $h_c/2 \leqslant h \leqslant h_c$.

C. Topological entropy and connectivity contribution

Our main quantity of interest is the classical topological entropy which we extract via the Levin-Wen scheme from the Rényi entropy. In order to reduce effects from asymmetries in the bipartition, we choose the thickness of any building blocks in the scheme to be $L/4$. We determine this entropy for a range of loop tensions $0 \leqslant h \leqslant 0.6$ since we expect it to reflect the phase transition at $h_c \approx 0.44$. For small system sizes we find a validation of the analytical expectation for the limits of $h \ll h_c$ and $h > h_c$ provided in Sec. III B with a continuous decrease of the topological entropy between the limiting values of $\ln 2$ and 0 around h_c (see Figs. 8 and 9). However, upon increasing L, an additional feature emerges in the range of $h_c/2 < h < h_c$, an interim overshooting of γ before it vanishes as expected near h_c. This overshooting converges to a plateau at a value of $2\ln 2$ for large L.

As discussed in Sec. III B, this overshooting is an artifact of the Rényi entropies with $n \geqslant 2$ and arises from the connectivity

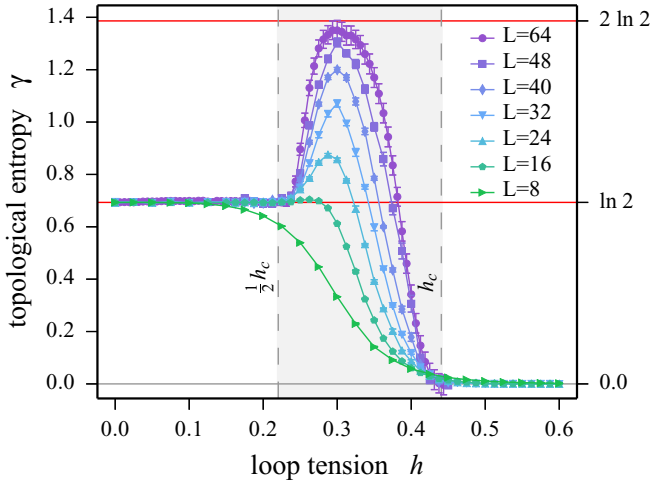

FIG. 8. (Color online) The $O(1)$ contribution to the Rényi entropy $S^{(2)}$ of the classical toric code model versus magnetic field/loop tension h determined via the Levin-Wen summation scheme. The $O(1)$ contribution contains the expected universal topological contribution of $\gamma = \ln(2)$ in the regime $h \leqslant h_c$ as well as an additional connectivity contribution $\gamma = \ln(2)$ in the intermediate regime $h_c/2 \leqslant h \leqslant h_c$ (indicated by the gray shaded area), in which for sufficiently large system sizes subsystem A already transitions into the paramagnetic phase.

contribution. Following the table of Fig. 4 we see that it yields a value of $2\ln 2$ for $n = 2$, to which the numerical data in Fig. 8 nicely converge.

$O(1)$ contributions for the 2D Ising model

The occurrence of this contribution evokes the question if it also arises in a system *without* topological order. For this reason, we numerically consider the 2D Ising model on the square lattice and extract the $O(1)$ contribution to the Rényi

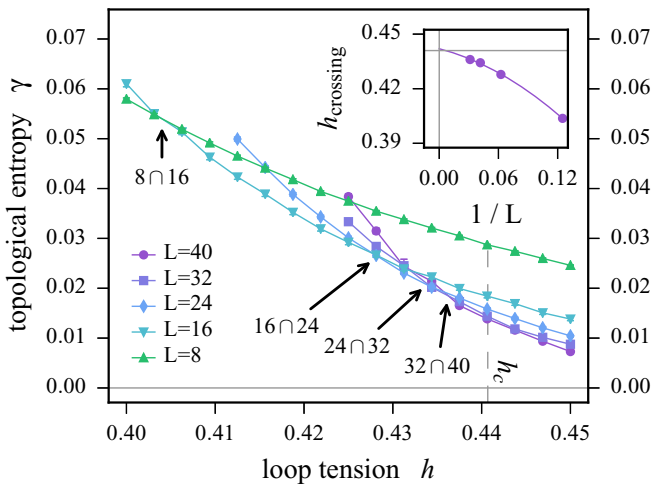

FIG. 9. (Color online) Near the critical loop tension, crossing points between data curves of different linear system sizes L can be identified. While keeping the difference between crossing L's constant ($\Delta L = 8$) a clear tendency towards the critical point can be observed upon increasing L. However, an extrapolation of the location of the crossing points is nontrivial because a subleading logarithmic contribution coming from corners of the subsystem is expected at criticality unlike in off-critical regions.

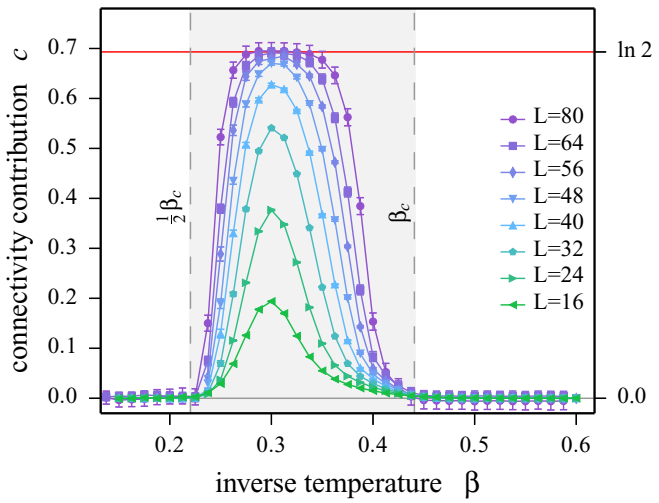

FIG. 10. (Color online) The $O(1)$ contribution to the Rényi entropy $S^{(2)}$ of the 2D Ising model versus inverse temperature β determined via the Levin-Wen summation scheme. While no topological contribution is expected, a finite $O(1)$ connectivity contribution of $\gamma = \ln(2)$ is observed in the intermediate regime $\beta_c/2 \leqslant \beta \leqslant \beta_c$ (indicated by the gray shaded area), in which for sufficiently large system sizes subsystem A already transitions into the low-temperature ordered phase.

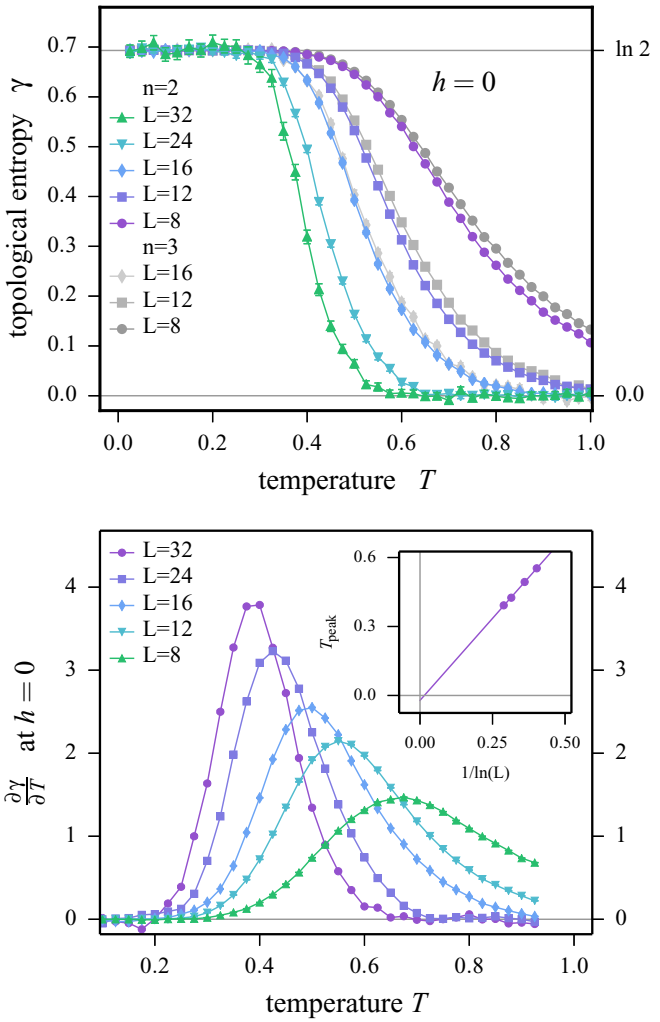

FIG. 11. (Color online) Top panel: finite-temperature behavior of topological entropy for the classical toric code model indicating the thermal transition from the low-temperature topologically ordered phase to the high-temperature paramagnet for various system sizes. Bottom panel: identification of the transition temperature into the topologically trivial phase by determining the peak position of the derivative $\partial\gamma/\partial T$ for various system sizes. The scaling of the so-determined transition temperatures shows the expected logarithmic scaling with system size indicating that topological order is unstable at finite temperature in the thermodynamic limit [35].

entropy when driving the Ising model through its thermal phase transition. Results are shown in Fig. 10 where we see the formation of a plateau at $\ln 2$ in the intermediate temperature regime between $\beta_c/2$ and β_c upon increasing system size. In this intermediate region, subsystem A already exhibits magnetic order. Since here we now allow for spontaneous symmetry breaking, the two possible magnetically ordered states contribute a term $\ln 2$ per disconnected part of subsystem A, i.e., $2\ln 2$ for bipartition A_1 and $\ln 2$ for bipartitions A_2, A_3, and A_4. Note that this is only the case if the disconnected parts of subsystem A are spatially separated beyond the correlation length, which explains the saturation on the plateau only for sufficiently large system sizes.

For higher Rényi entropies with $n \geqslant 2$ we thus expect a plateau at a level of $\ln 2/(n-1)$ between β_c/n and β_c in the thermodynamic limit.

D. Finite-temperature simulations

For finite temperatures, excitations that break the closed-loop constraint of the zero-temperature loop gas are thermally activated. These thermally induced defects, i.e., open loops in the configurations, are expected to drive the system into a disordered phase and hence destroy its topological order. In fact, in the thermodynamic limit it is known [35] that topological order does not survive for any finite temperature $T > 0$. For finite system sizes, however, a thermal crossover between the topologically ordered and the disordered phase takes place at some finite crossover temperature $T_{\mathrm{co}}(L)$. As pointed out in Ref. [35], the crossover temperature vanishes as $T_{\mathrm{co}}(L) \sim (\ln L)^{-1}$, both for the quantum and classical toric codes.

We verify this argument by numerically calculating the vanishing of the topological signature in the Rényi entropy via finite-temperature simulations, initially in the absence of a magnetic field, i.e., $h = 0$. Our results are depicted in Fig. 11 and clearly show the expected behavior, i.e., a vanishing of the topological entropy for sufficiently large temperatures. To determine the location of the actual crossover temperature, we identify the inflection points of the topological entropy (see the lower panel of Fig. 11). Indeed, the so-determined crossover temperatures show perfect $1/\ln L$ scaling.

At this point, one might ponder why no intermediate behavior appears for this transition (similar to the ones discussed before) given that the replica technique again puts the system effectively at β in part B and at 2β in part A. A related question is whether the crossover temperature indicates whether subsystem A or B loses its topological order. We

checked the latter by calcualting the next higher Rényi entropy $S_3(A)$, which puts part A at temperature 3β. As illustrated in Fig. 11, the crossover temperatures do not move at all, thus indicating that it occurs only when subsystem B undergoes the disorder transition.

This behavior can be qualitatively understood from considering, for instance, what happens to the boundary constraints for bipartition A_4 of the Levin-Wen summation scheme above the crossover temperature $T_{\rm co}$ (where subsystem A is still topologically ordered while subsystem B is not). Open loops can now traverse subsystem A such that the original closed-loop constraints for the two boundaries melt into a single constraint for the total boundary of part A. As a consequence, not only the topological ln 2 contribution of bipartition A_4 vanishes (cf. the table in Fig. 4), but also all connectivity contributions (which arise from a similar boundary counting argument).

Finite magnetic field

Finally, we turn to the combined effect of finite-temperature defects and loop tension in the toric code. For such a model, the statistical weights of a loop configuration σ become

$$w(\sigma) = \exp(-\beta J_v D_\sigma + \beta h m_\sigma), \tag{14}$$

where D_σ denotes the number of loop defects and m_σ is the total magnetization. Note that in contrast to the zero-temperature study above, we have now introduced an explicit temperature also in the weight stemming from a finite loop tension. In particular, this implies that if the temperature is too low compared to the loop tension h, there is no topological order since all fluctuations of the loop gas are frozen out from the loop tension and the configuration is a single trivial state (see Fig. 12). Only if $h \ll \beta^{-1} \ll J_v$, the system samples all loop configurations with approximately equal weight and topological order is observed. To this extent, $h_{\rm eff} = \beta h$ takes the role of an effective loop tension. Therefore, the left half of Fig. 12 shows precisely the same physics as Fig. 8 seen from right to left, including the occurrence of a connectivity contribution for an intermediate regime $h_c/2 < h_{\rm eff} < h_c$ of the effective loop tension. On the other hand, for sufficiently high temperatures we again start to thermally activate defects resulting in a thermal crossover where the topological entropy drops to zero (see the right half of Fig. 12). Again, we see that this crossover temperature vanishes like $1/\ln L$ with increasing system size, precisely mimicking the behavior seen for the system without magnetic field in Fig. 11.

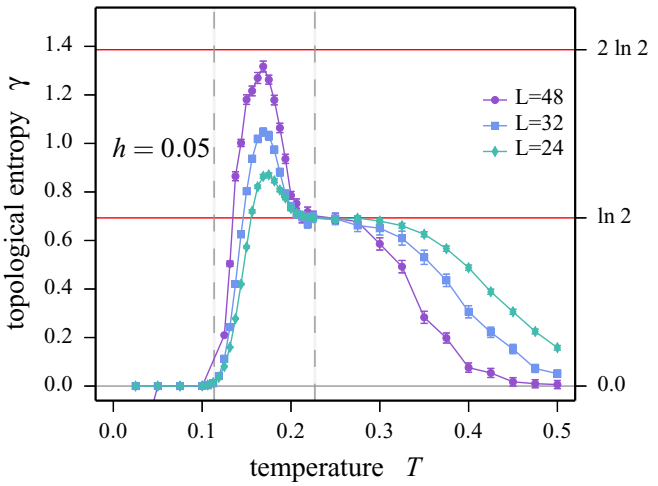

FIG. 12. (Color online) Finite-temperature behavior of $O(1)$ contribution to the Rényi entropy $S^{(2)}$ of the classical toric code model in the presence of a finite magnetic field/loop tension $h = 0.05$. The $O(1)$ contribution exhibits the expected universal topological contribution $\gamma = \ln(2)$, which contributes for sufficiently large temperatures and vanishes at high temperatures. An additional connectivity contribution of $\gamma = \ln(2)$ is observed in an intermediate regime. It can be understood from noting that the *effective* field is $h_{\rm eff} = \beta h$ as we introduced β in the Hamiltonian. Hence, this field increases for $T \to 0$ and we observe the same behavior as in Fig. 8 (read from right to left). The gray shaded area indicates the regime of $h_c/2 < h_{\rm eff} < h_c$. At very low temperature, even a small field $h = 0.05$ leads to the frozen trivial phase so that no topological order is present and thus $\gamma = 0$.

V. DISCUSSION

To summarize, we have studied the breakdown of topological order in classical many-body systems from a Rényi entropy perspective. One main result is the occurrence of an intermediate coupling regime, in which partial subsystem ordering leads to additional $O(1)$ contributions to the Rényi entropy, a scenario which we extensively discussed in the context of the classical toric code model.

While we have concentrated our discussion on the Levin-Wen summation scheme [5] to extract these $O(1)$ contributions, it is probably worthwhile to point out that all observations reported here analogously apply to the alternative Kitaev-Preskill summation scheme [6] as well. We note in passing that in applying the Kitaev-Preskill summation scheme to detect topological order in classical systems, one needs to (i) adapt a topologically nontrivial geometry for the bipartitions (e.g., a donut geometry) in contrast to the application for quantum systems and (ii) be aware of the fact that not all corner contributions are fully eliminated in this scheme [36].

A natural question is to ask is whether such effects may also occur in quantum systems. To this end, it is worth pointing out that the replica scheme to calculate the quantum Rényi entropies is defined in the worldline representation of the partition function, i.e., replicas are stitched together in imaginary time or inverse temperature. Thus, the reported artifacts would only occur when considering *thermal* phase transitions of quantum systems and would not be expected to occur for zero-temperature quantum phase transitions driven by some coupling parameter (which is not explicitly used in the replica representation).

On the other hand, we note that the classical Rényi entropies we discussed here are directly related [37] to the basis-dependent Shannon entanglement entropy introduced and studied in Refs. [38–40]. These basis-dependent Shannon and Rényi entropies as well as related quantities have been shown to exhibit unexpected additional signatures when driving a system through a phase transition [38,40], likely reflecting the same physics discussed here.

Taking an even wider perspective, we might think of our results as indications of the limitations of the Rényi entropies with regard to their $n = 1$ counterparts, i.e., the von

Neumann entanglement entropy and the classical Shannon entropy. Other limitations of the Rényi entropies have been discussed earlier, e.g., in the context of the $O(N)$ model [41] as well as Rokhsar-Kivelson–type wave functions [42–44], which both show additional (boundary) phase transitions for Rényi indices $n \geqslant 2$. In the latter case, the quantum entropy may be mapped onto a classical problem with different replicas stitched together, but all at the same temperature. Such a gluing can be sufficient to trigger an ordering, not in the bulk but at the boundary. In both cases, a precise renormalization group analysis is needed to address the possibility of an intermediate boundary phase transition. For generic, more complicated states such types of ordering may or may not occur; the precise behavior as a function of Rényi index n would (likely) need to be worked out case by case depending on the model and on spatial dimensionality. So far, all known examples refer to critical states without topological order in spatial dimension $d > 1$, which are driven away from criticality due to the gluing of several replicas. However, it appears unlikely that such a phenomenon could occur in gapped topologically ordered systems at zero temperature. Indeed, in that case no connectivity contribution has been observed in numerical simulations so far [30], even though these are typically limited to relatively small system sizes.

ACKNOWLEDGMENTS

We thank P. Calabrese, M. Hermanns, and A. Rosch for insightful discussions. S.T. thanks R. G. Melko for an inspiring exchange that has led to the idea for the calculations in the manuscript at hand. J.H. acknowledges support from the Bonn-Cologne Graduate School of Physics and Astronomy. Our numerical simulations were performed on the CHEOPS cluster at RRZK Cologne.

APPENDIX: REPLICA LOOP GAS SAMPLING

In this Appendix, we will provide a detailed account of the adaptation of nonlocal loop updates to the replica setup. The core of a Monte Carlo simulation is its implementation of the Markov chain of configurations, i.e., the algorithm for selecting and accepting new configurations. This is sketched in the following. The major challenge is that any configuration within the replica system has to satisfy the loop gas constraint in both replicas. Starting from a valid configuration, which could, e.g., be the state with all spins pointing down, we will apply a modification to this state by creating or deleting loops. To do so, we have the algorithm sample a *template loop*, a loop in the lattice which does not take care of the orientation of the spins. If accepted according to the detailed balance condition, this template loop will be applied to the spins along this loop by flipping them. This procedure is shown in Fig. 13. Sampling a template loop is particularly challenging if this loop crosses part A since its degrees of freedom are identified with those in the other replica. Thus, two additional open-loop ends are generated in the other replica at the boundary between A and B. These two ends need to be linked in part B of the other replica as well. Trying this, it is possible to cross part A again. Obviously, this procedure can easily result in a seesaw of linking two open-loop legs in part B of either replica.

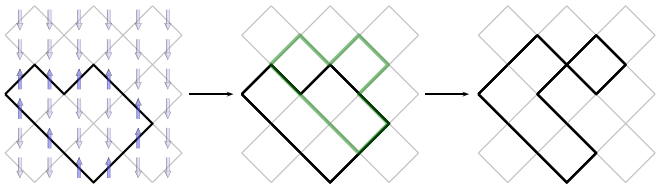

FIG. 13. (Color online) A loop update is performed by creating a template loop (green) in the lattice and applying it to the spin configuration with its spin loops (black) if the resulting energy change is accepted.

For the actual procedure of choosing the template loop, a first approach is to perform a random walk through the lattice. Once a valid loop is found, we apply a Metropolis probability between the current and the potential next state to decide on its acceptance. Later, we will present a more advanced algorithm which unifies the selection and acceptance step in a so-called directed walk.

By a walk we mean a procedure that creates a series of adjacent vertices whose links carry a spin. During the algorithmic creation of the series, the walk has a *head* which is the last appended vertex. This head "decides" which vertex (and thereby which spin) to append next.

1. Random walk

The random walk is started at an arbitrary vertex of the toric code lattice and proceeds with equal probability of $\frac{1}{4}$ to one of the four neighboring vertices [45]. Once a vertex is visited a second time, we can stop the walk and discard the first segment of the loop up to the first visit of this vertex. Possibly, the random walk has entered one or more times the connected subregion A so that its segments in A in the other replica also have to be included in the template loop. Thus, an even number of open template loop ends is created in the other replica at the boundary to part B. To match these ends, it is efficient to start individual random walks at every open end simultaneously. If the head of one of the walks hits a vertex already visited by a different walk, we have created a linking loop between the two open ends so that these two are *healed*. Most likely, the two loops do not meet precisely at their heads so that a superfluous part between the meeting point and one of the heads arises. This part of the template loop is discarded (cf. Fig. 14). It may also happen that a specific random walk head hits a vertex twice. In this case, we can discard the resulting *internal* loop of this walk since it does not help in linking open ends. Moreover, the general strategy is to keep the total length of the template loop as short as possible.

In Monte Carlo parlance, this procedure is responsible for ensuring ergodicity in our simulation. What remains is to fulfill also detailed balance. Since we have only generated a template loop so far, we can compare the total weight of the configuration prior to the application of this template loop and after it. In our special case we need to determine the magnetizations m_{before} and m_{after}. The acceptance is then decided on by the Metropolis probability

$$p(\sigma \to \sigma \circ \text{template loop}) = \min(1, e^{h(m_{\text{after}} - m_{\text{before}})}), \quad \text{(A1)}$$

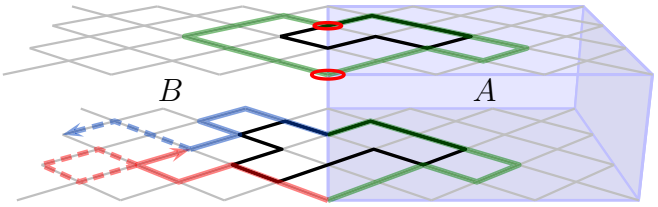

FIG. 14. (Color online) Visualization of the healing process. On top, a template loop (green) is sampled within the first replica. It leaves behind two open loop ends (red circles) at the boundary between A and B in the other replica. The right sketch depicts the healing processes: two random walks (blue and red) simultaneously try to meet each other. The dashed segments indicate parts of the template loops which are discarded. Internal loops (dashed red) would be allowed but are contracted in order to shorten the total template loop.

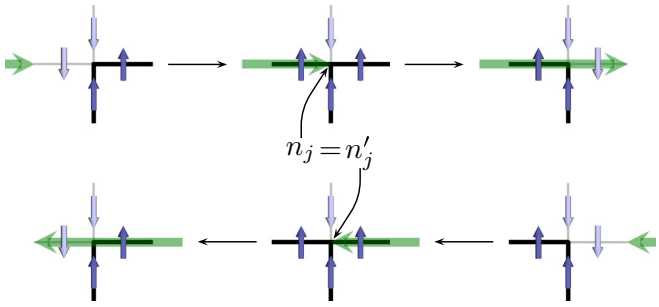

FIG. 15. (Color online) Passing of the directed walk (green) at vertex j. The normalization constants for inverse loop update walks agree. In this example, they both have the value of $n_j = 3\exp(-h) + \exp(h)$.

where the function composition symbol $\circ$ is used to denote the application of the template loop on the current configuration.

Since this implementation of the Markov chain separates the selection and acceptance of new configuration, we can almost freely design the random walk procedure as long as we guarantee ergodicity. A shortcoming of it appears at higher loop tension h where the acceptance of an energetically less favorable configuration is low. In addition, for relatively large sizes of the subsystem A, the healing of all open-loop ends can entail many random walks back and forth between the replicas. This makes the algorithm less efficient, especially for parameter settings ($h \approx 0.44$, L large) we want to investigate to track the phase transitions.

2. Directed walk

A substantially different and more efficient approach for the Monte Carlo update scheme is implemented by unifying selection and acceptance. The idea is to ensure detailed balance on-the-fly while choosing the template loop. Strictly speaking, it is no longer a *template* loop since all spins along this loop are flipped with probability 1, i.e., they can (and have to) be flipped directly. The walk that the head of the loop performs is not at random but obeys probability rules depending on the value of the potential next spins to be visited. In general, the rule is to select the next spin (which unambiguously selects the next vertex) with so-called heat bath probability. This means the microscopic weights w_i of all candidates for the next head of the loop are added up to a normalization constant n. In the toric code model, the head has four possibilities to choose the next spin because bouncing must now be included. The only possible values for the weights are $w_i \in \{\exp(h), \exp(-h), \exp(2h), \exp(-2h)\}$, where the factor of 2 in the exponent applies in the connected part A which is simulated at an effective loop tension of $2h$ as discussed above. With the constant $n = \sum_{i=1}^{4} w_i$ the heat bath probabilities for the four directions are defined as

$$\frac{w_1}{n}, \frac{w_2}{n}, \frac{w_3}{n}, \frac{w_4}{n}. \tag{A2}$$

It is not obvious to see whether this rule generates an update which obeys the detailed balance condition. To check it, we need to identify a reverse update to any (completed) update and compare the probabilities of their occurrence. If we now try to fractionize this update into its individual moves according to the heat bath rule and compare it to its reverse move (cf. Fig. 16), we see that the normalization constants thwart the analysis: A specific spin at position j in the loop was chosen to be visited (and flipped) with probability w_j/n_j in the original update. Doing its reverse, we would have the probability w_j^{-1}/n'_{j+1} to reflip it. The ratio of the two probabilities is in general not w_j/w_j^{-1} as they should be from the ratio of the weights of the configurations that differ by flipping spin j. Two facts about the involved normalization constants annoy: (i) they originate from different configurations and (ii) they are shifted by a lattice position.

We see that issue (i) is not a problem by realizing that the value of normalization constant at a specific vertex at the moment when it is the head is the same for both, the original and its reverse, update is the same, i.e. $n_j = n'_j$. This can be understood from Fig. 15 where we see that the coming-from and the going-to spin switch roles (and weights) in both situations.

The other issue (ii) can be resolved by leaving the local perspective from the loop head and regarding the entire loop update. If we consider a chain of moves and its reversion, we have to multiply all probabilities to obtain the total probability for the walk. In the ratio of the total probabilities for the walk and its reverse, we realize that all normalization constants vanish. Since their respective numerator-denominator pairing is shifted by one in the product, we dub this feature of the microscopic rule *staggered detailed balance*. The staggering can be seen in Fig. 16 and the ratio between a loop update and its reverse is given later in Eq. (A4).

We have seen that detailed balance can be satisfied in principle by the design of the walk but crucial aspects have not been discussed yet: How is a loop initiated and finished and what are the decision rules for choosing the next spin at the boundary between A and B? It is clear that a loop must bifurcate when leaving part A, but how is a reunification at another site at the boundary accepted? The latter may fail such that the update is discarded for technical reasons (as opposed to probabilistic reasons).

For the start of a loop update, a random spin in a random replica is chosen and one of its adjacent vertices is selected with probability of $\frac{1}{2}$. This spin is immediately flipped and

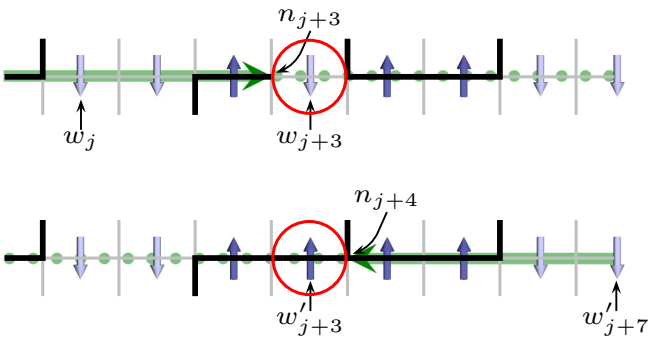

FIG. 16. (Color online) Formation of the probabilities of two reversing update loops at a specific intermediate position $j+3$ of the walk using heat bath probabilities. We compare the probabilities of selecting the encircled spin in the right-moving loop and in its reversal left-moving counterpart. The probability in the right-moving case is $w_{j+3}/n_{j+3} = \exp(h)/[\exp(-h) + 3\exp(h)]$. Note that spins at $j \ldots j+2$ are already flipped when the loop does this selection at n_{j+3} since we perform the update in place. For the reverse move the selection probability is $w'_{j+3}/n_{j+4} = \exp(-h)/[3\exp(-h) + \exp(h)]$. In particular, the ratio of these to probabilities is *not* $\exp(2h)$ as it should be if we wanted a microscopic detailed balance for the spin flip at $j+3$.

the walk continues at the selected vertices following the heat bath rule. It is instructive to note at this point that we have not "paid" the flipping of this first spin in terms of acceptance probabilities. This will be caught up at the decision to end the loop. The probability to start the loop at a particular pair of a spin and a vertex is thus simply

$$p_{\text{init}} = \frac{1}{4N}, \tag{A3}$$

where N is the total number of spins in the lattice.

In order to finish the walk, it is first of all necessary that the loop is closed, i.e., that the head reaches precisely the other vertex at the initial spin (the vertex that was *not* chosen to start with). This is not sufficient since just like anywhere the head is free at this vertex to choose any of the adjacent spins, among them the initial spin. Before we determine the heat bath probabilities and normalization constant we have to flip the initial spin once again. The loop head thus "sees" the original orientation of this spin before the whole loop update was started. Afterwards, the heat bath selection is performed and in the case the initial spin is chosen, it is flipped a third time and the loop update is successfully finished. Only now, the flipping of the initial spin is justified ("paid") by a probabilistic selection according to its weight. If another but the initial is chosen, the loop continues and we must not forget to flip the initial spin again.

We have now explained the algorithm for non-boundary-crossing loops. Figure 17 and the following equation prove that the detailed balance condition is fulfilled:

$$\frac{p(\sigma \to \sigma')}{p(\sigma' \to \sigma)} = \frac{p_{\text{init},s_0} \frac{w_{s_1}}{n_1} \frac{w_{s_2}}{n_2} \cdots \frac{w_{s_{l-1}}}{n_{l-1}} \frac{w_{s_0}}{n_l}}{\frac{w_{s_0}^{-1}}{n_1} \frac{w_{s_1}^{-1}}{n_2} \cdots \frac{w_{s_{l-2}}^{-1}}{n_{l-1}} \frac{w_{s_{l-1}}^{-1}}{n_l} p_{\text{init},s_0}} = \frac{w(\sigma')}{w(\sigma)}. \tag{A4}$$

The relative shift of the numerators again demonstrates what we mean by staggered detailed balance for the loop steps. The

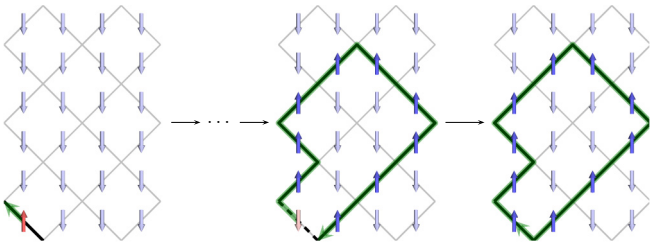

FIG. 17. (Color online) Completing a loop by catching up the probabilistic choice of the initial spin as part of the loop. The initial spin is drawn red in order to emphasize that it was not *paid* in terms of probabilistic weight selection until the last step. In the middle sketch it is temporarily flipped back since the loop head must choose it as if it was never flipped.

chronological order of the appearance of the probabilities is from left to right in the main numerator but from right to left in the main denominator. We chose to write the equation in this way to emphasize the reversing effect of factors that are written one below the other.

It remains to define rules how to deal with boundary crossings and their resulting bifurcations of the loop. In order to justify the probabilities for the direction of the walk we need to ensure reversibility of any moves we allow. This is the reason why we only allow a single bifurcation of the loop and hope for its reunification. In case the reunification fails, the update is aborted and the original configuration is restored. We will elucidate this point further at the end of this section. The vertices of interest for the treatment of boundary crossings are those which have adjacent spins in either of the bipartitions, subsequently called *boundary vertices*. In general, we will never set a heat bath normalization constant at a vertex using weights from both parts, i.e., both $\exp(\pm h)$ and $\exp(\pm 2h)$. In other words, a drift to or away from the connected part A is avoided.

We first describe the update for the case of an initial spin somewhere in part B. If a boundary vertex is visited coming from the disconnected part B we treat all four spins as if they were in part B (although at least one is in part A) for the calculation of the heat bath weights. In other words, the head does not *see* the boundary. If the head selects a spin in part A, also its counterpart in the other replica is flipped. However, the flipping of this counterpart is at that state not paid in terms of acceptance probability just as we used this wording above. The loop continues in part A where it uses the weights $\exp(\pm 2h)$ until it reaches again a boundary vertex. At such an occurrence, we have to perform the mentioned bifurcation: first, a loop is continued in the initially chosen replica only. This loop should now rejoin the initial spin in the same way we described above for the simpler case devoid of a connected part A. Trying this, the loop must not enter part A again. If it does, we have to abort the entire update. Second, another loop is continued in the respective other replica. In the same manner, this loop is expected to rejoin the by then unpaid spin in part A at the entering boundary spin. To successfully finish the total loop update, this unification must happen without a prior visit of part A again. Figure 18 illustrates the described procedure.

A slight difference needs to be made if the initial spin of the update is part A. In this case, the first visit of a boundary vertex leads to bifurcation and the first bifurcated loop in one

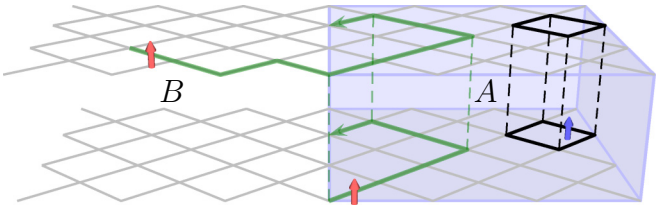

FIG. 18. (Color online) In the presence of a connected subsystem A loops need to bifurcate. After entering part A, all weights have to be taken using the effective loop tension of $2h$ and flipped in both replicas. The first spin in part A in the other at the entrance is unpaid (drawn red), just like the initial spin in part B. The bifurcation happens when the loop leaves part A again and must be finished individually in both replicas by joining the red spins.

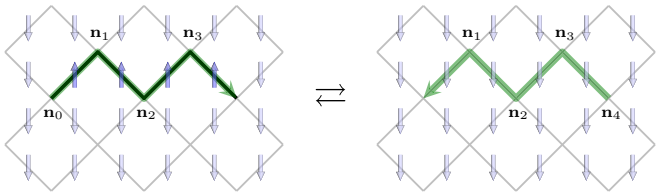

FIG. 19. (Color online) Two mutually reversing open-loop updates including the normalization constants used for the respective choice of the next direction of the walk. The last normalization n_4 (resp. n_0) is missing and therefore will be included artificially in the decision to stop the loop.

of the replicas in part B is free to reenter part A at any boundary vertex. Not before the second bifurcated loop in part A is performed and rejoins the unpaid boundary spin that its counterpart has been selected for reentering part A, the subsequent loop in part A is continued and hopefully rejoins the initial spin.

Our implementation of the Monte Carlo algorithm resigns to allow multiple temporary open loops in part B in one of the replicas alone. In principle, one could allow more than one open loop and perform the loop update in the initial replica until it rejoins the initial spin. Subsequently, one could start to connect all $2n_o$ open ends in part B of the other replica. Doing so it would be important to start the connecting walks only at those n_o ends that arose from *leaving* part A in the initial replica. Special care must be taken in this approach to not mix the order of the start spins of the healing walks in part B of the other replica. They must be started in the same order they arose from the initial loop. This is due to the ambiguity of possible paths that lead to the same loop update. Mixing the order of starting spins would violate the detailed balance condition because the reversal loop of a loop could then be achieved through more than one move.

We decided to allow only a single pair of bifurcations of the loop and avoid long seesaw healing processes for a single update step.

3. Finite-temperature simulations

So far, we have considered the classical toric code at zero temperature, i.e., the system subjected to the loop gas constraint. By releasing this constraint and activating the vertex terms in the Hamilton function (8) we investigate the toric code at finite temperature. In this situation, pairs of open-loop ends are permitted at the energetical cost of two times the vertex coefficient J_v. In practice, we set $J_v = 1$ since only the ratio between J_v and h is important. A loop update in our Monte Carlo simulation must therefore be able to introduce open loops. Once again, we propose two strategies.

Our first approach consists of separating the operations of the loop update and the introduction of loop excitations. We pick two vertices of the total system at random and have the algorithm perform a random walk between them. At $h = 0$ we only need to determine an acceptance probability for the open ends, which we set to Boltzmann weights $\exp(\pm J_v)$ or $\exp(\pm 2J_v)$ depending on the subsystem where the open end is introduced. In case one of the vertices is in part A and the other in part B, we need a third vertex in part B of the respective other replica and thus create a "double-tongued" open loop. Also, at finite loop tension we can apply Metropolis probabilities to the acceptance of a sampled open loop by balancing both the change in energy and in magnetization between the current and the proposed configurations.

Going beyond the simple sampling technique we also present an algorithm that again includes the acceptance probability in the selection of the subsequent configuration. We therefore extend our zero-energy algorithm based on heat bath selections for the random walk at every vertex in the lattice. The head of the loop may take four different directions at a specific vertex. We add a fifth event to these four, namely, stopping the loop and thereby creating (or annihilating) an open-loop end in the spin configuration. However, we will not include the decision of stopping the loop in the heat bath sum but perform it separately using the Boltzmann weight of an open-loop end. This decision is made prior to the selection of the next bond to walk on. There is one issue concerning the detailed balance between an open-loop update and its reversal update: Due to the staggered detailed balance philosophy, the last heat bath normalization constant of the walk does not enter any of the probabilities for the loop continuation but the first one does (see Fig. 19). Roles are switched in the reversal update, which implies that the two normalization constants at the edges do not vanish in the ratio between the opposite loop updates.

Our workaround is to artificially include every heat bath normalization constant (and thus also the last one) into the decision of stopping the loop. The probability to stop at the $j$ths vertex of the loop is thus $\frac{\exp(\pm J_v)}{n_j}$. Since in our model $n_j > 1$ in any case it cannot happen that this alteration of the pure Boltzmann constant leads to trivial probabilities (>1) for stopping the loop. In formulas, the ratio between two opposing loop updates is given by

$$\frac{p(\sigma \to \sigma')}{p(\sigma' \to \sigma)} = \frac{p_{\mathrm{init},v_0} w_{v_0} \frac{w_{s_0}}{n_0} \left(1 - w_{v_1}\right) \frac{w_{s_1}}{n_1} \left(1 - w_{v_2}\right) \ldots \left(1 - w_{v_{l-1}}\right) \frac{w_{s_{l-1}}}{n_{l-1}} \frac{w_{v_l}}{\boldsymbol{n_l}}}{\frac{w_{v_0}^{-1}}{\boldsymbol{n_0}} \frac{w_{s_0}^{-1}}{n_1} \left(1 - w_{v_1}\right) \frac{w_{s_1}^{-1}}{n_2} \left(1 - w_{v_2}\right) \ldots \left(1 - w_{v_{l-1}}\right) \frac{w_{s_{l-1}}^{-1}}{n_l} w_{v_l}^{-1} p_{\mathrm{init},v_l}} = \frac{w(\sigma')}{w(\sigma)}. \tag{A5}$$

Until now, we have neglected again the bipartition and replication of the lattice. But, surprisingly the situation becomes easier if open loops are allowed. We can simply forbid boundary crossings of open loops, i.e., abort a loop update which tries it. The algorithm is nevertheless ergodic since an arbitrary loop update (including a boundary crossing) can by generated by two noncrossing open loops which share one of their ends at the boundary. Moreover, also closed loops can be created that way by creating an open loop whose starting and ending vertices coincide. This does not make the closed-loop algorithm superfluous since it is indispensable at the hard loop gas constraint and more efficient for very low temperature in combination with the open-loop algorithm.

[1] L. Balents, Spin liquids in frustrated magnets, Nature (London) **464**, 199 (2010).

[2] For a recent review, see e.g. J. Eisert, M. Cramer, and M. B. Plenio, Colloquium: Area laws for the entanglement entropy, Rev. Mod. Phys. **82**, 277 (2010).

[3] J. D. Bekenstein, Black Holes, and Entropy, Phys. Rev. D **7**, 2333 (1973); S. W. Hawking, Particle Creation by Black Holes, Commun. Math. Phys. **43**, 199 (1975).

[4] M. A. Metlitski and T. Grover, Entanglement entropy of systems with spontaneously broken continuous symmetry, arXiv:1112.5166.

[5] M. Levin and X. G. Wen, Detecting Topological Order in a Ground State Wave Function, Phys. Rev. Lett. **96**, 110405 (2006).

[6] A. Kitaev and J. Preskill, Topological Entanglement Entropy, Phys. Rev. Lett. **96**, 110404 (2006).

[7] While the topological entanglement entropy is a powerful indicator of topological order, it does not allow to fully identify the topological quantum field theory (TQFT) underlying this order. An example of such an ambiguity are the TQFTs for the toric code and the double semion theory, which both lead to a topological entropy of $\gamma = 2\ln 2$.

[8] H.-C. Jiang, Z. Wang, and L. Balents, Identifying topological order by entanglement entropy, Nat. Phys. **8**, 902 (2012).

[9] S. Depenbrock, I. P. McCulloch, and U. Schollwöck, Nature of the Spin-Liquid Ground State of the S=1/2 Heisenberg Model on the Kagome Lattice, Phys. Rev. Lett. **109**, 067201 (2012).

[10] C. Castelnovo and C. Chamon, Topological order and topological entropy in classical systems, Phys. Rev. B **76**, 174416 (2007).

[11] M. Hermanns and S. Trebst, Rényi entropies for classical string-net models, Phys. Rev. B **89**, 205107 (2014).

[12] A. Y. Kitaev, Fault-tolerant quantum computation by anyons, Ann. Phys. (NY) **303**, 2 (2003).

[13] H. A. Kramers and G. H. Wannier, Statistics of the two-dimensional ferromagnet, Phys. Rev. **60**, 252 (1941).

[14] S. Trebst, P. Werner, M. Troyer, K. Shtengel, and C. Nayak, Breakdown of a Topological Phase: Quantum Phase Transition in a Loop Gas Model with Tension, Phys. Rev. Lett. **98**, 070602 (2007).

[15] L. Onsager, Crystal Statistics. I. A Two-Dimensional Model with an Order-Disorder Transition, Phys. Rev. **65**, 117 (1944).

[16] For completeness, it should be mentioned that this mapping is strictly defined for the even parity sector of the toric code model. Other parity sectors of the toric code would necessitate the definition of antiperiodic boundary conditions in the Ising model for every odd winding number in the toric code model.

[17] C. Holzhey, F. Larsen, and F. Wilczek, Geometric and renormalized entropy in conformal field theory, Nucl. Phys. B **424**, 443 (1994).

[18] P. Calabrese and J. Cardy, Entanglement entropy and quantum field theory, J. Stat. Mech. (2004) P06002.

[19] P. B. Buividovich and M. I. Polikarpov, Numerical study of entanglement entropy in SU(2) lattice gauge theory, Nucl. Phys. B **802**, 458 (2008); Y. Nakagawa, A. Nakamura, S. Motoki, and V. I. Zakharov, Entanglement entropy of SU(3) Yang-Mills theory, PoS (**LAT2009**), 188 (2009).

[20] M. B. Hastings, I. Gonzalez, A. B. Kallin, and R. G. Melko, Measuring Rényi Entanglement Entropy in Quantum Monte Carlo Simulations, Phys. Rev. Lett. **104**, 157201 (2010).

[21] N. M. Tubman and J. McMinis, Renyi entanglement entropy of molecules: Interaction effects and signatures of Bonding, arXiv:1204.4731.

[22] C. M. Herdman, Stephen Inglis, P.-N. Roy, R. G. Melko, and A. Del Maestro, Path-integral Monte Carlo method for Rényi entanglement entropies, Phys. Rev. E **90**, 013308 (2014).

[23] T. Grover, Entanglement of Interacting Fermions in Quantum Monte Carlo Calculations, Phys. Rev. Lett. **111**, 130402 (2013); P. Broecker and S. Trebst, Rényi entropies of interacting fermions from determinantal quantum Monte Carlo simulations, J. Stat. Mech. (2014) P08015.

[24] L. Wang and M. Troyer, Rényi Entanglement Entropy of Interacting Fermions Calculated Using the Continuous-Time Quantum Monte Carlo Method, Phys. Rev. Lett. **113**, 110401 (2014).

[25] J. E. Drut and W. J. Porter, A hybrid Monte Carlo approach to the entanglement entropy of interacting fermions, Phys. Rev. B **92**, 125126 (2015).

[26] A. J. Daley, H. Pichler, J. Schachenmayer, and P. Zoller, Measuring Entanglement Growth in Quench Dynamics of Bosons in an Optical Lattice, Phys. Rev. Lett. **109**, 020505 (2012); Dmitry A. Abanin and Eugene Demler, Measuring Entanglement Entropy of a Generic Many-Body System with a Quantum Switch, *ibid.* **109**, 020504 (2012); S. J. van Enk and C. W. J. Beenakker, Measuring $\mathrm{Tr}\rho^n$ on Single Copies of ρ Using Random Measurements, *ibid.* **108**, 110503 (2012).

[27] R. Islam, R. Ma, P. M. Preiss, M. E. Tai, A. Lukin, M. Rispoli, M. Greiner, Measuring entanglement entropy through the interference of quantum many-body twins, arXiv:1509.01160

[28] J. Iaconis, S. Inglis, A. B. Kallin, and R. G. Melko, Detecting classical phase transitions with Renyi mutual information, Phys. Rev. B **87**, 195134 (2013).

[29] J. Cardy and I. Peschel, Finite-size dependence of the free energy in two-dimensional critical systems, Nucl. Phys. B **300**, 377 (1988).

[30] S. V. Isakov, M. Hastings, and R. G. Melko, Topological Entanglement Entropy of a Bose-Hubbard Spin Liquid, Nat. Phys. **7**, 772 (2011).

[31] R. G. Melko, A. B. Kallin, and M. B. Hastings, Finite-size scaling of mutual information in Monte Carlo simulations: Application to the spin-$\frac{1}{2}$ XXZ model, Phys. Rev. B **82**, 100409(R) (2010).

[32] S. Humeniuk and T. Roscilde, Quantum Monte Carlo calculation of entanglement Rényi entropies for generic quantum systems, Phys. Rev. B **86**, 235116 (2012).

[33] A. W. Sandvik, Stochastic series expansion method with operator-loop update, Phys. Rev. B **59**, R14157 (1999); O. F. Syljuasen and A. W. Sandvik, Quantum Monte Carlo with directed loops, Phys. Rev. E **66**, 046701 (2002); O. F. Syljuasen, Directed loop updates for quantum lattice models, *ibid.* **67**, 046701 (2003); F. Alet, S. Wessel, and M. Troyer, Generalized directed loop method for quantum Monte Carlo simulations, *ibid.* **71**, 036706 (2005).

[34] J.-M. Stéphan, S. Inglis, P. Fendley, and R. G. Melko, Geometric Mutual Information at Classical Critical Points, Phys. Rev. Lett. **112**, 127204 (2014).

[35] C. Castelnovo and C. Chamon, Entanglement and topological entropy of the toric code at finite temperature, Phys. Rev. B **76**, 184442 (2007).

[36] M. Hermanns (private communication).

[37] This connection can be most easily seen for the mutual information of an infinite strip or cylinder, cut into two parts, and expressing the Shannon mutual information in the transfer matrix formalism (see, e.g., Ref. [34]), one is led to a particular basis that allows the definition of a Shannon entropy of the ground state. For general Rényi index $n \geqslant 2$ such a relation can also be established.

[38] F. C. Alcaraz and M. A. Rajabpour, Universal Behavior of the Shannon Mutual Information of Critical Quantum Chains, Phys. Rev. Lett. **111**, 017201 (2013).

[39] J.-M. Stéphan, Shannon and Rényi mutual information in quantum critical systems, Phys. Rev. B **90**, 045424 (2014).

[40] F. C. Alcaraz and M. A. Rajabpour, Universal behavior of the Shannon and Rényi mutual information of quantum critical chains, Phys. Rev. B **90**, 075132 (2014).

[41] M. A. Metlitski, C. A. Fuertes, and S. Sachdev, Entanglement Entropy in the O(N) model, Phys. Rev. B **80**, 115122 (2009).

[42] J.-M. Stéphan, G. Misguich, and V. Pasquier, Rényi entropy of a line in two-dimensional Ising models, Phys. Rev. B **82**, 125455 (2010).

[43] J.-M. Stéphan, H. Ju, P. Fendley, and R. G. Melko, Entanglement in gapless resonating-valence-bond states, New. J. Phys. **15**, 015004 (2013).

[44] A. Chandran, V. Khemani, and S. L. Sondhi, How Universal is the Entanglement Spectrum?, Phys. Rev. Lett. **113**, 060501 (2014).

[45] Except for the first step, the respective precursor in the walk can be excluded from the choice (avoid bouncing) so that the probability is $\frac{1}{3}$ for the remaining directions.